# **CHAPTER 162**

# Numerical Model for Longshore Current Distribution on a Bar-Trough Beach

# Yoshiaki KURIYAMA<sup>1</sup>

## Abstract

A numerical model for the time-averaged nearshore current in the surf zone is developed to simulate the longshore current distribution on a bar-trough beach that has a peak velocity shoreward of the bar crest. Momentum fluxes due to mass transport under broken waves, which are ignored in other models, are included in the present model. The validity of the model is verified with field data.

## 1. Introduction

There are two patterns of the time-averaged longshore current distribution on a bar-trough beach. One has a peak velocity seaward of the bar crest, and the other has the peak shoreward of the bar crest. Kuriyama and Ozaki (1993) measured longshore current velocities in the field when a single bar-trough system was formed and waves broke over the bar. They showed that eighty-five percent of the measured longshore current distributions have peak velocities shoreward of the bar crests, whereas fifteen percent have peaks seaward of the bar crests.

The seaward peak can be reproduced by one-dimensional models of the longshore current where the driving force of the longshore current is the cross-shore gradient of radiation stress (Ebersole and Dalrymple, 1980; Larson and Kraus, 1991) because the gradient is largest seaward of a bar crest owing to the large dissipation of wave energy due to wave breaking. On the other hand, the shoreward peak cannot be reproduced by the one-dimensional models. Church and Thornton (1993) and Smith et al. (1993) have recently developed one-dimensional numerical models for the longshore current that include the effect of turbulence due to wave breaking on the driving force through consideration of the surface roller. Although the peak velocities predicted by their models are located shoreward of the peaks predicted by previous

<sup>1)</sup> Senior Research Engineer, Port and Harbour Research Institute Nagase 3–1–1, Yokosuka, Kanagawa 239, JAPAN

models, the peaks predicted by their models are still located seaward of the peaks measured in the field. Symonds and Huntley (1980) showed that the longshore gradient of wave setup can cause a shoreward peak. The shoreward peak, however, was sometimes observed when the longshore gradient of the wave setup was small.

The objective of this study is to develop a numerical model that reproduces the shoreward peak in the longshore current even when the longshore gradient of the wave setup is small. It is assumed that the momentum fluxes due to mass transport under broken waves generate the shoreward peak, and the resultant momentum fluxes are introduced into a previous nearshore current model. Longshore current distributions predicted by the present model are compared with those measured in the filed.

#### 2. Numerical Model

The present model consists of two computationally distinct numerical models: a wave height transformation model and a nearshore current model.

2.1 Wave height transformation model

The present model for wave height transformation is based on the Karlsson's model (1969) for directional random waves, which is based on the balance of wave energy. I introduce a wave energy dissipation term as Takayama et al. (1991) did. The energy equation of a wave component with the frequency of f and the direction of  $\theta$  is expressed as

$$\frac{\partial (D_s V_x)}{\partial x} - \frac{\partial (D_s V_y)}{\partial y} + \frac{\partial (D_s V_{\theta})}{\partial \theta} = -D,$$

$$D_s = S(f, \theta) \delta f \delta \theta,$$

$$V_x = C_g \sin \theta, V_y = C_g \cos \theta,$$

$$V_{\theta} = \frac{C_g}{C} (-\cos \theta \frac{\partial C}{\partial x} - \sin \theta \frac{\partial C}{\partial y}),$$
(1)

where  $D_s$  is the wave energy, S is the directional wave spectral density,  $\delta f$  is the frequency band width,  $\delta \theta$  is the directional band width,  $C_g$  is the group velocity, C is the celerity, and D is the wave energy dissipation rate. The values of  $D_s$ ,  $C_g$ , C and D are defined for a wave component. The co-ordinate system used in this paper is shown in Figure 1. The positive direction of the y-axis is seaward. The wave direction is defined relative to the shoreward direction and positive counterclockwise. The vertical axis extends upward.

The principle of the dissipation term proposed by Dally et al. (1985) is used in the present model because the dissipation term can reproduce the wave height stabilization in a uniform depth, which is like the wave transformation over a trough.

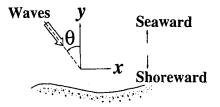


Figure 1 Definition sketch of co-ordinate system.

Modification of the dissipation term by Dally et al., which is for one-dimensional monochromatic waves, yields Eq. (2) for a wave component of directional random waves.

$$D = \frac{K}{h} (D_{S}C_{g} - D_{S}\frac{E_{S}}{E}C_{g}),$$

$$E_{S} = \frac{1}{16} \rho g (H_{1/3})_{S}^{2}, \quad (H_{1/3})_{S} = \Gamma h.$$
(2)

where  $(H_{1/3})_s$  is the stable significant wave height, h is the still water depth, E is the total wave energy, the sum of  $D_s$ ,  $E_s$  is the total energy where the wave height is stable after wave breaking, and K and  $\Gamma$  are dimensionless empirical coefficients.

I assume that K and  $\Gamma$  are functions of the beach slope, tan  $\beta$ , and express them with Eqs.(3) and (4) because the wave energy dissipation in the surf zone is affected by the beach slope. These functions were obtained on the basis of the calculations of the wave height transformation in the surf zone for offshore wave steepness of 0.02 by Goda (1975).

$$K=1.7 \times 10^{\alpha}, \ \alpha = -0.857 \log_{10}(1/\tan\beta) + 0.219.$$
 (3)

$$\Gamma = -0.14 \log_{10}(1/\tan\beta) + 0.56.$$
<sup>(4)</sup>

The significant wave height,  $H_{1/3}$ , and the principal wave direction,  $\theta_p$ , are calculated by

$$H_{1f3} = 4.0 \sqrt{m_0}, \ m_0 = \int_0^\infty \int_{-2/\pi}^{2/\pi} D_s d\theta \, df.$$
 (5)

$$\theta_p = \int_0^\infty \int_{-2/\pi}^{2/\pi} \theta D_s d\theta \, df/\, m_0. \tag{6}$$

The significant wave period,  $T_{1/3}$ , is assumed to be equal to that in deep water.

## 2.2 Nearshore current model

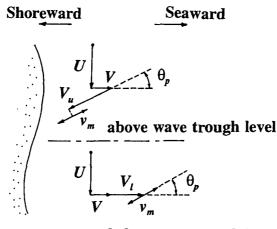
#### a. Momentum equation

The movements of water particles, which have the maximum orbital velocity of  $v_m$  due to waves, are assumed as shown in Figure 2. Water particles above the wave trough level,  $d_{ur}$ , are transported by the depth and time-averaged nearshore current; U and V are the longshore and cross-shore components of the nearshore current velocity. The particles are also transported shoreward by mass transport due to waves at the angle of  $\theta$  and the velocity of  $V_u$ . Water particles below the wave trough level are transported by the nearshore current, and transported seaward at the velocity of  $V_l$  of the return flow, which is perpendicular to the shore. The mass of water transported shoreward by the mass transport is assumed to be equal to that transported seaward by the return flow.

Under the assumptions, the cross-shore flux of the longshore momentum in the surf zone,  $M_w$ , is expressed as

$$M_{w} = \frac{\rho}{T} \int_{0}^{T} \int_{d_{r}}^{\eta} [\{U + (V_{u} + v_{m} \cos \sigma t) \sin \theta_{p}\} \\ \{V + (V_{u} + v_{m} \cos \sigma t) \cos \theta_{p}\}] dz dt$$

$$+ \frac{\rho}{T} \int_{0}^{T} \int_{-h}^{d_{r}} [(U + v_{m} \cos \sigma t \sin \theta_{p}) \\ (V + V + v_{m} \cos \sigma t \sin \theta_{p})] dz dt$$
(7)



below wave trough level

Figure 2 Definition sketch of the assumed movements of water particles above and below the wave trough level.

where  $\rho$  is the density of sea water, T is the wave period,  $\eta$  is the elevation of water surface, z is the upward elevation relative to the mean water level,  $\sigma$  is the angular frequency. The value of  $T_{I/3}$  is used as T in the calculation.

Equation (7) becomes

$$M_{w} = \frac{\rho}{T} \int_{0}^{T} \left\{ \int_{-h}^{\eta} UV dz + \int_{-h}^{\eta} v_{m}^{2} \cos^{2} \sigma t \sin \theta_{p} \cos \theta_{p} dz + \int_{-h}^{\eta} v_{m}^{2} \cos^{2} \sigma t \sin \theta_{p} \cos \theta_{p} dz + U \left( \int_{d_{r}}^{\eta} V_{u} \cos \theta_{p} dz + \int_{-h}^{d_{r}} V_{l} dz \right) + \int_{d_{r}}^{\eta} \left( V_{u}^{2} + VV_{u} \right) \sin \theta_{p} \cos \theta_{p} dz \right\} dt.$$

$$(8)$$

The first and second terms on the right-hand side of Eq.(8) represent the momentum flux due to the nearshore current and a radiation stress, respectively. The third term is equal to zero because the mass of water transported shoreward is assumed to be equal to that transported seaward. The fourth term is the cross-shore flux of the longshore momentum due to mass transport by waves.

In most previous models for the nearshore current, the fourth term is neglected because the effect of the mass transport due to unbroken waves on the nearshore eurrent is small. However, the mass flux under broken waves is several times of that calculated with a formula for unbroken waves (Nadaoka and Kondoh, 1982). This means that a momentum flux due to mass transport under broken waves is much greater than that under unbroken waves. Therefore I eonsider that the momentum fluxes due to mass transport under broken waves are significant for the prediction of the longshore eurrent distribution on a bar-trough beach, and introduce the fluxes into a previous model.

The fourth term,  $M_{bI}$ , becomes Eq.(9) with a surface roller model proposed by Svendsen (1984) as shown in Figure 3; in his model, a water particle in the surface roller is transported shoreward with the eelerity, C,

$$M_{hl} \doteq \rho P_{h} e \left( -C \cos \theta_{n} + V \right) C \sin \theta_{n}, \tag{9}$$

where e is the time-averaged thickness of the surface roller, and  $P_b$  is the fraction of breaking waves, which is introduced for random waves. The value of e is assumed as

$$e = C_A H_{1/3}^2 / L, (10)$$

in which  $C_A$  is a dimensionless coefficient, and L is the wavelength for the wave period of T.

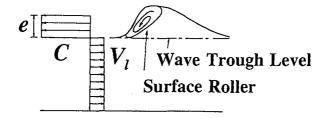


Figure 3 Definition sketch of the vertical distribution of time-averaged crossshore velocity in a surface roller model by Svendsen (1984).

The cross-shore flux of the cross-shore momentum due to broken waves,  $M_{b2}$ , and the longshore flux of the longshore momentum,  $M_{b3}$ , are obtained in a similar way for the value of  $M_{b1}$ ; these are described by

$$M_{b2} = \rho P_b e C^2 \cos^2 \theta_p + (d_{tr} + h) V_l^2.$$
<sup>(11)</sup>

$$M_{b3} = \rho P_b e(C \sin \theta_p + 2U) C \sin \theta_p.$$
(12)

The value of  $V_i$  is expressed as Eq.(13), which is derived by Kuriyama(1991) on the basis of Svendsen's model (1984).

$$V_{l} = (C \frac{m_{0}}{h^{2}} + P_{b} C_{A} \frac{H_{1/3}^{2}}{hT}) \cos\theta_{p}.$$
 (13)

Finally, the horizontal momentum equations in the present model for the nearshore current, which contains the momentum fluxes due to surface rollers, are represented by

$$\frac{\partial U}{\partial t} + U \frac{\partial U}{\partial x} + V \frac{\partial U}{\partial y} + F_x - L_x + R_x + g \frac{\partial \overline{\eta}}{\partial x} + M_x = 0,$$

$$\frac{\partial V}{\partial t} + U \frac{\partial V}{\partial x} + V \frac{\partial V}{\partial y} + F_y - L_y + R_y + g \frac{\partial \overline{\eta}}{\partial y} + M_y = 0,$$
(14)

$$L_{x} = \frac{\partial}{\partial x} \left( \epsilon \frac{\partial U}{\partial x} \right) + \frac{\partial}{\partial y} \left( \epsilon \frac{\partial U}{\partial y} \right), L_{y} = \frac{\partial}{\partial x} \left( \epsilon \frac{\partial V}{\partial x} \right) + \frac{\partial}{\partial y} \left( \epsilon \frac{\partial V}{\partial y} \right),$$

$$R_{x} = \frac{1}{\rho(h + \overline{\eta})} \left( \frac{\partial S_{xx}}{\partial x} + \frac{\partial S_{yx}}{\partial y} \right), R_{y} = \frac{1}{\rho(h + \overline{\eta})} \left( \frac{\partial S_{xy}}{\partial x} + \frac{\partial S_{yy}}{\partial y} \right),$$

$$M_{x} = \frac{1}{\rho(h + \overline{\eta})} \left( \frac{\partial M_{b3}}{\partial x} + \frac{\partial M_{b1}}{\partial y} \right), M_{y} = \frac{1}{\rho(h + \overline{\eta})} \left( \frac{\partial M_{b1}}{\partial x} + \frac{\partial M_{b2}}{\partial y} \right),$$
(15)

where  $\overline{\eta}$  is the elevation of the mean water level,  $F_x$  and  $F_y$  are the bottom friction terms,  $L_x$  and  $L_y$  are the lateral mixing terms,  $S_{xx}$ ,  $S_{xy}$ , and  $S_{yy}$  are the radiation stress components, and  $\epsilon$  is a lateral mixing coefficient. The subscripts x and y denote the values in the x-direction and y-direction.

#### b. Fraction of breaking waves

Seaward of a bar crest, I assume that the fraction of breaking waves is a function of wave height-water depth ratio as Thornton and Guza (1983) did, and represent it by Eq.(16) with a dimensionless coefficient,  $\gamma$ , which is the wave height-water depth ratio in the surf zone, where all waves are broken.

$$P_{b} = \{H_{1/3} / (\gamma h)\}^{4} . \tag{16}$$

I introduce the effect of beach slope into the calculation of  $\gamma$  because the wave energy dissipation in the surf zone depends on beach slope. The value of  $\gamma$  is assumed as Eq.(17) on the basis of the calculations of the wave height in the surf zone for offshore wave steepness of 0.02 by Goda (1975).

$$\gamma = 0.68 \exp(4.2 \tan \beta)$$
. (17)

Shoreward of a bar crest, the fraction of breaking waves is assumed as

$$P_{b} = (P_{b})_{bar}, \qquad y_{bar} - 10 < y \le y_{bar},$$

$$P_{b} = (P_{b})_{bar} - 0.014(y - y_{bar} + 10)^{2}, \quad y \le y_{bar} - 10,$$
(18)

where  $(P_b)_{bar}$  is the fraction of breaking waves at the bar crest, and  $y_{bar}$  is the offshore distance at the bar crest. According to visual observations, waves break even shoreward of a bar crest. This means that the fraction of breaking waves does not decrease rapidly from a bar crest although the value predicted by Eq.(16) decreases rapidly from the bar crest. Thus, the fraction of breaking waves shoreward of a bar crest is assumed to be constant near the bar crest and to decrease shoreward proportionally to the square of the distance from the shoreward limit of the constant  $P_b$  zone. The coefficients of Eq.(18) were determined on the basis of visual observation data (Kuriyama and Ozaki, 1993); the units of y and  $y_{bar}$  are meters.

Near the surf zone shoreward of a trough, Eq.(16) is used again where  $P_b$  estimated by Eq.(16) is larger than that by Eq.(18).

## c. Surface roller area parameter, $C_A$

I assume that  $C_A$  changes according to the development and decay of the surface roller although it is treated as a constant value by Svendsen (1984), because a constant  $C_A$  cannot represent the disappearance of the surface roller in a trough. The development and decay of the surface roller are assumed to be proportional to the fraction of wave breaking; the maximum value of  $C_A$  is determined to be 4.0 on the basis of the field data obtained by Kuriyama (1991). Finally,  $C_A$  is expressed as

$$C_{A} = 4.0 P_{h}.$$
 (19)

d. Radiation stress, bottom shear stress and lateral mixing

The radiation stresses of directional random waves are calculated by Eq.(20) proposed by Yamaguchi(1988).

$$S_{xx} = \int_{0}^{\infty} \int_{-\pi/2}^{\pi/2} \rho g \left\{ \frac{C_g}{C} \sin^2 \theta + \left( \frac{C_g}{C} - \frac{1}{2} \right) \right\} D_s d\theta df,$$

$$S_{xy} = S_{yx} = \int_{0}^{\infty} \int_{-\pi/2}^{\pi/2} \rho g \left\{ \frac{C_g}{C} \cos \theta \sin \theta D_s d\theta df,$$

$$S_{yy} = \int_{0}^{\infty} \int_{-\pi/2}^{\pi/2} \rho g \left\{ \frac{C_g}{C} \cos^2 \theta + \left( \frac{C_g}{C} - \frac{1}{2} \right) \right\} D_s d\theta df.$$
(20)

Equation (21) (Nishimura, 1982; Nishimura, 1988) is used for the calculation of the bottom shear stresses,  $F_x$  and  $F_y$ . The value of 0.005 is used as the friction coefficient,  $C_f$ .

$$F_{x} = \rho C_{f} \{ (W + \frac{w_{b}^{2}}{W} \sin^{2}\theta_{p}) U - \frac{w_{b}^{2}}{W} \sin\theta_{p} \cos\theta_{p} V \},$$

$$F_{y} = \rho C_{f} \{ \frac{w_{b}^{2}}{W} \sin\theta_{p} \cos\theta_{p} U - (W + \frac{w_{b}^{2}}{W} \cos^{2}\theta_{p}) V \},$$

$$W = \{ \sqrt{U^{2} + V^{2} + w_{b}^{2} + 2(U \sin\theta_{p} - V \cos\theta_{p}) w_{b}} + \sqrt{U^{2} + V^{2} + w_{b}^{2} + 2(U \sin\theta_{p} - V \cos\theta_{p}) w_{b}} \} / 2,$$

$$w_{p} = 2 (v_{m})_{b} / \pi, \quad (v_{m})_{b} = \frac{\pi H_{1/3}}{T \sin(2\pi h/L)}.$$
(21)

The lateral mixing coefficient proposed by Battjes (1975) is used in the present model. This coefficient is given by

$$\epsilon = Mh(\frac{D_{total}}{\rho})^{1/3}, \qquad (22)$$

where  $D_{total}$  is the total wave energy dissipation rate and M is a dimensionless eoefficient. Lateral mixing is probably related to turbulence; the turbulence due to breaking waves is much larger than that due to non-breaking waves. Hence, the degree of the lateral mixing in a trough is expected to be smaller than that in the surf zone loeated shoreward of the trough. Although the lateral mixing coefficient proposed by Longuet-Higgins (1970) is widely used, it seems to be inappropriate for the prediction of the longshore current on a bar-trough beach because the coefficient proposed by Longuet-Higgins, which is proportional to the distance from the shoreline, does not reproduce the difference between the lateral mixing in a trough and that in the shoreward surf zone. On the other hand, the lateral mixing coefficient proposed by Battjes reproduces the difference because it is based on the wave energy dissipation due to wave breaking. Thus, in the present model, I adopt the lateral mixing coefficient proposed by Battjes.

## 3. Model Comparisons with Measurements

The significant wave heights and the longshore current velocities predicted by the present model are compared with the values measured at Hazaki Oceanographical Research Facility (HORF), which is a field observation pier of 427m in length on the Kashima-nada coast of Japan facing to the Pacific Ocean. Water surface elevations were measured with ultrasonic wave gages before and after the measurement of the longshore current. A spherical float having a diameter of 0.2m was used to measure time-averaged longshore current velocities 1m below the water surface. This method with the float was confirmed to be useful for the measurement of the time-averaged longshore current velocity by calibrations with an electromagnetic eurrent meter; there is a strong correlation between the time-averaged longshore current velocity measured by the float and that measured by the current meter (Kuriyama and Ozaki, 1993).

## 3.1 Calculation conditions

The ealculation results for three cases, on March 24, 28 and April 4, 1989, are compared with the measurements. Figure 4 shows the topographic map of the vicinity of the HORF on March 31; this topography is used in the calculations for the three eases because the beach profile changes from March 24 to April 4 were small. The topography was almost uniform alongshore although seour occurred around the tip and the middle of the HORF, y=380m and y=200m, where piles are concentrated. The calculation areas extend from the shorelines to y=650m, and alongshore from x=-320m to x=320m.

In the calculations of wave height transformation, the grid distances in x-direction and y-direction are 10m. The numbers of frequency components and directional components are 10 and 35, respectively. The wave heights,  $(H_{1/3})_{ob}$ , the wave periods,  $(T_{1/3})_{ob}$ , the principal wave directions,  $(\theta_p)_{1/3}$ , and the spreading parameters,  $(s_{max})_{ob}$ , input at the offshore boundaries are listed in Table 1. The Bretschneider-Mitsuyasu frequency spectrum and the Mitsuyasu-type spreading function are given at the offshore boundaries.

In the calculations of wave energy dissipation, a beach slope below 1/100 and that over 1/10 are replaced by values of 1/100 and 1/10, respectively, because Eqs.(3) and (4) are valid for the beach slopes from 1/100 to 1/10.

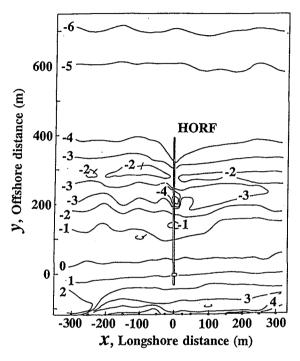


Figure 4 Topographic map of the vicinity of the HORF.

Table 1 Offshore boundary conditions	Table 1	Offshore	boundary	conditions
--------------------------------------	---------	----------	----------	------------

Case	Date	(H <sub>1/3</sub> ) <sub>ob</sub>	(T <sub>1/3</sub> ) <sub>ob</sub>	$(\theta_p)_{ob}$	(S <sub>max</sub> ) <sub>ob</sub>
1	March 24	3.20m	11.20s	-20.0°	90
2	March 28	2.47m	8.86s	-25.0°	40
3	April 4	2.03m	8.40s	-10.0°	45

The nearshore currents are calculated with the horizontal momentum equations, Eqs.(14) and (15), and the continuity equation by the ADI (Alternating Direction Implicit) method. The calculations are done for 4000 time step with a step length of 0.4s; the grid distances are 10m.

The nearshore current velocities are assumed to be equal to zero at the offshore boundaries and at the shorelines. The nearshore current velocities and the mean water levels at the side boundaries are assumed to be equal to the values at internal grid points next to the side boundaries.

The longshore flux of the longshore momentum,  $M_{b3}$ , is neglected in the calculations of the nearshore current because the nearshore currents preliminarily calculated by a previous model are almost uniform alongshore.

#### 3.2 Wave height

Figures 5 shows the predicted significant wave heights and the values measured at the HORF. The solid lines show the values predicted by the present model, and the closed circles show the values measured before and after the measurements of the longshore current. The predicted values agree well with the measured values except for the data near the shorelines.

Causes of the small disagreement of calculated and measured values near the shorelines are supposed to be infragravity waves and the increase of water depth due to wave setup. When an offshore wave height is large, the amount of wave setup and the infragravity wave height are large near the shoreline. Infragravity waves and the increase of water depth due to wave setup, however, are not taken into account in the present model although the gradient of mean water level is considered in the nearshore current model. Disregard of the two factors results in the disagreement of calculated and measured values near the shorelines.

#### 3.3 Nearshore current

Figure 6 shows a comparison of the longshore current velocities measured at the HORF with those predicted by the present model and by a previous model, which does not include momentum fluxes due to mass transport under broken waves; the velocities on March 24 and 28 were predicted with M=5 and those on April 4 were predicted with M=10. Seaward of the bar crests, the values predicted by the present model and by the previous model increase shoreward; both agree with the measured values. Shoreward of the bar crests, however, the values predicted by the present model and the measured values increase toward shore whereas the values predicted by the present the troughs predicted by the present model agree well with the measured values whereas the values predicted by the present model agree well with the measured values whereas the values predicted by the previous model by the present model agree well with the measured values whereas the values predicted by the previous model of the previous model agree well with the measured values whereas the values predicted by the previous model agree well with the measured values whereas the values predicted by the previous model agree well with the measured values whereas the values predicted by the previous model do not.

The Longshore current velocities predicted by a quasi-present model where the fraction of breaking waves shoreward of the bar crest is estimated with Eq.(16) are also shown in Figure 6. The peaks in velocity predicted by the quasi-present model are located at the bar crests, shoreward of the peaks predicted by the previous model and seaward of the peaks measured at the HORF and predicted by the present model.

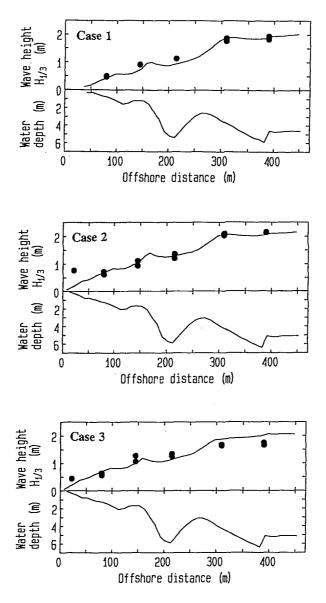


Figure 5 Comparison of the significant wave heights measured at the HORF (circles) with those predicted by the present model.

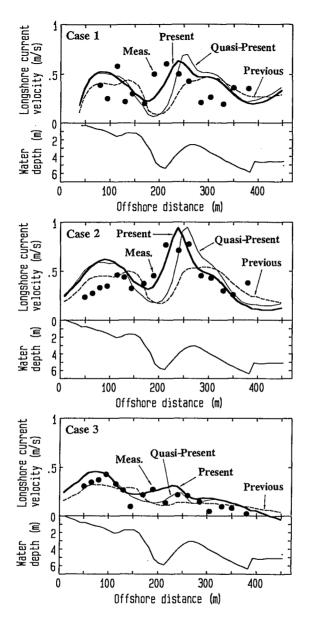


Figure 6 Comparison of the longshore current velocities measured at the HORF (circles) with those predicted by the previous model (broken lines), by the quasi-present model (thin solid lines), and by the present model (thick solid lines).

## 4. Discussion and Conclusions

Let us assume that an incident wave angle and the longshore current velocity are positive. Shoreward of a bar crest, the cross-shore flux of the longshore momentum due to the surface roller decreases with travel shoreward owing to the decay of the roller. This decrease means that the cross-shore flux of the longshore momentum transported into a unit volume is larger than that transported out of the volume. Consequently the longshore current velocities calculated by the present model are larger than those calculated by the previous model.

On the other hand, seaward of the bar crest, the cross-shore flux of the longshore momentum due to the surface roller increases with travel shoreward owing to the development of the surface roller. Thus the longshore current velocities calculated by the present model are smaller than those calculated by the previous model. As a result, the longshore current distribution calculated by the present model has a peak velocity shoreward of the bar crest.

The longshore current distributions predicted by the quasi-present model have peaks at the bar crests, seaward of the peaks predicted by the present model because the surface roller calculated by the quasi-present model with Eq.(16) decays rapidly from the bar crest whereas the roller calculated by the present model with Eqs.(16) and (18) propagates without decay near the bar crest, and then gradually decays.

The longshore current distributions on a bar-trough beach predicted by the present model agree with the field measurements, which have peaks in velocity shoreward of the bar crests, better than the distributions predicted by the other two models. The agreement shows that the fraction of breaking waves predicted by Eq.(18) is reasonable shoreward of a bar crest and the momentum fluxes due to mass transport under broken waves are significant for the prediction of the longshore current.

#### Acknowledgement

The author would like to thank Mr. Yasushi Ozaki for analyzing field data. Further acknowledgement is extended to Dr. Nicholas C. Kraus, Director of Conrad Blucher Institute, Texas A&M University -Corpus Christi, for his useful comments that improved this paper.

#### References

- Battjes J. A. (1975): Modeling of turbulence in the surf zone, Symp. on Modeling Techniques, ASCE, pp.1050-1061.
- Church J. C. and E. B. Thornton (1993): Effects of breaking wave induced turbulence within a longshore current model, Coastal Eng., 20, pp.1-28.
- Dally W. R., R. G. Dean and R. A. Dalrymple (1985): Wave height variation across beaches of arbitrary profile, J. Geophys. Res., Vol.90, No.C6, pp.11,917– 11,927.
- Ebersole B. A. and R. A. Dalrymple (1980): Numerical modeling of nearshore circulation, Proc. 17th Coastal Eng. Conf., pp.2710-2725.

- Goda Y. (1975): Irregular wave deformation in the surf zone, Coastal Eng. in Japan, Vol.18, pp.13-26.
- Karlsson T. (1969): Refraction of continuous ocean wave spectra, J. Waterways and Harbors Div., Proc. of the ASCE, Vol.95, No.WW4, pp.437-448.
- Kuriyama Y. (1991): Investigation of cross-shore sediment transport rates and flow parameters in the surf zone using field data, Rep. of the Port and Harbour Res. Inst., Vol.30, No.2, pp.3-58.
- Kuriyama Y. and Y. Ozaki (1993): Longshore current distribution on a bar-trough beach -Field measurements at HORF and numerical model-, Rep. of the Port and Harbour Res. Inst., Vol.32, No.3, pp.3-37.
- Larson M. and N. C. Kraus (1991): Numerical model of longshore current for bar and trough beaches, J. Waterway, Port, Coastal, and Ocean Eng., Vol.117, No.4, ASCE, pp.326-347.
- Longuet-Higgins M. S. (1970): Longshore current generated by obliquely incident waves, 1&2, J. Geophys. Res., Vol.75, No.33, pp.6778-6801.
- Nadaoka K. and T. Kondoh (1982): Laboratory measurements of velocity field structure in the surf zone by LDV, Coastal Eng. in Japan, Vol.25, pp.125-146.
- Nishimura H. (1982): Numerical simulation of the nearshore circulation, Proc. 29th Japanese Conf. on Coastal Eng., JSCE, pp.333-337. (in Japanese)
- Nishimura H. (1988): Computation of nearshore current, Nearshore Dynamics and Coastal Process – Theory, Measurements and Predictive Models – (ed. by K. Horikawa), University of Tokyo Press, pp.271–291.
- Smith J. M., M. Larson and N. C. Kraus (1993): Longshore current on a barred beach: Field measurements and calculation, J. Geophys. Res., Vol.98, No.C12, pp.22717-22731.
- Svendsen I. A. (1984): Mass flux and undertow in a surf zone, Coastal Eng., 8, pp.347-365.
- Symonds G. and D. A. Huniley (1980): Waves and currents over nearshore bar systems, Proc. of Canadian Coastal Conf., pp.64-78.
- Takayama T., N. Ikeda and T. Hiraishi (1991): Practical computation method of directional random wave transformation, Rep. of the Port and Harbour Res. Inst., Vol.30, No.1, pp.21-67. (in Japanese)
- Thornton E. B. and R. T. Guza (1983): Transformation of wave height distribution, J. Geophys. Res., Vol.88, No.C10, pp.5925-5938.
- Yamaguchi M. (1988): A numerical model of nearshore currents due to irregular waves, Proc. of 21st Coastal Eng. Conf., ASCE, pp.1113-1126.